IEEE Access
Multidisciplinary | Rapid Review | Open Access Journal

Received 6 December 2023, accepted 13 January 2024, date of publication 16 January 2024, date of current version 24 January 2024.

Digital Object Identifier 10.1109/ACCESS.2024.3355013

APPLIED RESEARCH

Quasi-Resonant Flyback Converter in an 800 V Inductive Charging System: Abnormal Operation and Control Aspects

DARKO Đ. VRAČAR, (Senior Member, IEEE)
BRUSA Elektronik (München) GmbH, 81829 Munich, Germany
e-mail: darko.vracar@brusa.biz

This work was supported by BRUSA Elektronik (München) GmbH, Munich, Germany; www.brusa.biz.

ABSTRACT This paper studies quasi-resonant flyback (QRF) dc-dc converter 57 W with valley-switching mode (VSM) in an emerging application. The QRF was supplied from variable 800 V input and was used as the auxiliary power supply of an inductive charging system. When choosing switch rated voltage it was shown that one shall consider maximum voltage during short-circuits too. Influence of high temperatures on transformer magnetizing inductance were analyzed and showed why this shall be considered when evaluating different vendors and designs. Operational waveforms are simulated and measured showing that key quantities were matched. Comprehensive overview of QRF abnormal operations is presented for the first time covering start-up, short-circuit, and over-power cases, including experiments. It was demonstrated that when solving noise-related start-up problem, by increasing filtering capacitance, one got positive influence on QRF operation (e.g. switching-frequency range was reduced, efficiency increased, and control loop bandwidth, phase margin and gain margin got improved). The short-circuits were evaluated through nine test-cases. When QRF operated in VSM the short-circuit protection worked as expected. But, if short-circuit happened at non-regulated output, at no load, it may go undetected—which is dangerous. Hence several mitigation strategies were proposed to prevent damage of converter. Also, for converters with variable switching frequency one shall state whether efficiency measurements were done when load was increasing or decreasing thus considering influence of controller's hysteresis. The transition thresholds, which ensure VSM operation, presented as ''input power vs. input voltage'', showed non-linear dependence.

INDEX TERMS Bode plots, control, dc-dc converter, efficiency, over-power protection, quasi-resonant flyback, short-circuit protection, start-up, thermal tests, transformer, transition thresholds.

NOMENCLATURE

ACF	Active-clamped flyback.
APS	Auxiliary power supply.
DCM	Discontinuous-conduction mode.
EMI	Electro-magnetic interference.
HV	High-voltage.
IC	Integrated circuit.
ICS	Inductive charging system.
OPP	Over-power protection.
QRF	Quasi-resonant flyback.
RCD	Resistor-capacitor-diode.
SiC	Silicon-carbide.
SCP	Short-circuit protection.
VSM	Valley-switching mode.
ZCD	Zero-crossing detection.

The associate editor coordinating the review of this manuscript and approving it for publication was Madhav Manjrekar.

I. INTRODUCTION

Since number of battery electric vehicles worldwide is increasing [1], with increased adoption pace too [2], so are research activities on inductive charging systems (ICS) of their batteries [3]. Majority of literature was covering, e.g., power conversion, efficiency improvements, compensation techniques, control, coil design, protection methods, etc. [4]. The first publications that were covering auxiliary power

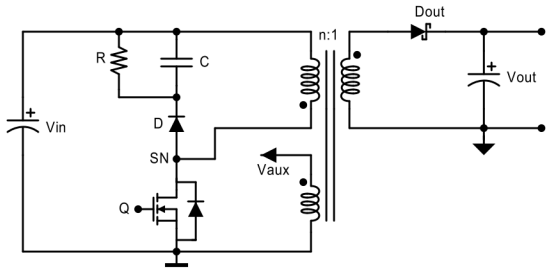

FIGURE 1. The QRF generic schematics with one output.

supplies (APS) of the primary, i.e. ground, side of ICS were [5], [6], [7], [8], and [9]. In [5], [6], [7], [8], and [9] the active-clamped flyback (ACF) dc-dc converter was used as an APS whilst in [4] the quasi-resonant flyback (QRF) dc-dc converter was analyzed. The detailed description of the 11 kVA ICS from BRUSA, where those APS were used, are given in [10] and [11].

In this paper we will investigate some design and control aspects as well as abnormal operation, when the QRF dc-dc converter 57 W, with valley-switching mode (VSM), is used as an APS of the primary side of the ICS 11 kVA. The aim of this paper is to present missing theoretical, simulation, and experimental results for the QRF in this emerging application that were not covered in [4].

Note that this paper introduces neither a new topology nor a control method, but analyzes usage of the known topology in an emerging application thus presents new knowledge. However, the findings presented here are applicable for any QRF with VSM or even to any kind of flyback or isolated dc-dc converters. Furthermore, a balance between practical and academic contributions is made thus making it usable for readers from industry and academia. Since this work is part of a commercial project not all design details may be presented.

The variable-frequency valley-switching QRF converter is a known topology since a long time [12]. In text it will be referred as "QRF with VSM" or QRF only. Its usual application is either as a power supply adapter [13] or auxiliary power supply [14]. The general analysis, operation, and design of a QRF are well explained in [15], [16], [17], [18], [19], and [20], hence will not be repeated. The small-signal analyses, that are relevant for this kind of converters, are covered in [20], [21], and [22].

The generic schematic of a QRF with valley-switching is shown in Fig. 1. We see that, from topology viewpoint, it is not different from a conventional flyback converter. But, a QRF with VSM is different in a sense that a circuit, which measures voltage of auxiliary winding (V_{aux}) on primary side, is introduced. Purpose of that circuit is to detect zero-crossing of the switch drain-voltage, i.e. the instant when energy from transformer is depleted. After that, a signal for turn-on of the switch Q is given, ensuring valley-switching thus reducing the switching losses and electro-magnetic interference (EMI) [23]. The SN in Fig. 1 denotes switching node—which is drain-source voltage of the switch Q.

A. KEY CONTRIBUTIONS

The original or novel contributions are listed as follows.

- When choosing switch rated voltage of a flyback converter one would typically consider maximum input voltage and reflected output voltage. Here it is shown that the peak drain-source voltage, during short-circuits at QRF converter outputs, shall be considered too. An appropriate procedure is introduced.
- Comparison of transformers' $L_m(I)$ (magnetizing inductance vs. primary current) characteristics with temperatures up to 120°C showed that above 100°C, depending on vendors' construction, differences may happen with significant inductance loss, although at 25°C they were comparable. Hence this aspect shall be considered when choosing vendors or comparing different designs.
- Comprehensive overview of QRF abnormal operation presented for the first time covering start-up, short-circuit, and over-power cases.
- When QRF was powered from the rectified mains voltage, randomly it was not able to start, but remained in an auto-restart mode. The reason was too much noise on ZCD/OPP pin [23] which forced QRF into fault-mode. The solution was simply to increase its filtering capacitance (C_{OPP})—which then influenced efficiency and Bode diagrams in a positive way.
- Short-circuit operation of QRF with multiple outputs was analyzed in detail with total of 9 test-cases for the first time. The short-circuit protection (SCP) was working as expected in VSM mode. However, when short-circuit happens at no load and at non-regulated output it may go undetected—which is dangerous. So appropriate mitigation strategies were proposed with goal to prevent that transformer burns or some other parts explode.
- The over-power protection (OPP) was analyzed in more detail than in [4]. A guide is given for the key-parts' choice for that circuit and importance of choice of filtering capacitor C_{OPP} on the ZCD/OPP pin of the controller NCP1340 [23]. It was discovered that value of C_{OPP} has impact on converter start-up, when supplied from rectified mains voltage, as well as on VSM, hence efficiency, and Bode plots.
- Operational waveforms are simulated and measured showing that voltages and primary currents were well matched. The matching was better than in [4].
- The efficiency graphs are plotted for QRF, with two different transformers and C_{OPP}values, showing huge difference. Increasing this capacitance increased the converter efficiency too.
- Since QRF operates with variable switching frequency, one shall state whether efficiency measurements were done when load was increasing or decreasing. Due to hysteresis in control IC the efficiency of QRF will be different depending on load's direction change.

- Graphs of QRF losses at no-load, for two transformers, were analyzed showing quadratic dependency of losses vs. input dc voltage. But no-load losses were not the key design parameter in this application.
- Thermal measurements with significantly increased gate resistor (100 Ω vs. 16 Ω) showed that temperature rise of the switch was only 6°C, i.e. switching losses did not increase too much. But that was beneficial to the reduction of EMI. Also, long-term temperature measurements of QRF in ICS were presented, for the first time, demonstrating good performance.
- The switching-frequency change was presented for QRF with different values of C_{OPP} demonstrating that increasing of C_{OPP} reduces switching-frequency range.
- The power transition thresholds, which ensure that QRF enters VSM operation, represented as an "*input power vs. input voltage*", are shown with higher number of considered input voltages than in [4]. As a result, one could see non-linear dependence (vs. linear one in [4]), and that difference between used regulated outputs 5.5 V was not so big anymore. Also, unwanted behavior was noticed at 850 V and light load (< 20 W) in a sense that QRF enters kind of transition mode between DCM (discontinuous-conduction mode) and pulse-skip mode. It seems that this is inherent to how NCP1340 [23] controller works and cannot be improved by end user.
- Bode plots were measured for QRF in VSM with increased filtering capacitance on ZCD/OPP pin (C_{OPP}) showing that simulated and measured results are better matched when compared to results in [4]. Also, it was noticed that bandwidth, phase margin, and gain margin values and ranges are now much better when compared to the results with smaller C_{OPP}.

II. DESIGN ASPECTS

In this section only some specific aspects of the QRF in ICS application will be analyzed. The general design considerations for the power stage are the same as for any conventional flyback dc-dc converter [5] and can be found in relevant datasheets of used control ICs, application notes or references [15], [16], [17], [18], [19], and [20].

A. CONVERTER DATA

The basic data of the 57 W QRF is given in Table 1. They are slightly different to the ACF presented in [5], [6], and [8] since the QRF had limited maximum switching frequency (vs. limited minimum switching frequency with ACF) and lower minimum dc input voltage (e.g. 240 V vs. 460 V). The latter feature made QRF universally applicable to majority of grids worldwide, i.e. single-, split-phase, and three-phase mains.

The QRF has two input-voltage ranges. One for the ICS power-transfer mode (PT) and another one for the ICS stand-by mode (SB). This was one of the challenges specific to the ICS application in general [5], [6], [8].

TABLE 1. The QRF data.

Parameter	Value
Input dc voltage (ICS power transfer)	620–880 V
Input dc voltage (ICS stand-by)	240–640 V
Output 1: voltage	+ 5.5 V
Output 1: load current	0.7 A
Output 2: (regulated) voltage	+ 5.5 V
Output 2: load current	2.5 A
Output 3: voltage	+ 22 V
Output 3: load current	1.74 A
Output 4/5: voltage	± 11 V
Output 4/5: load current	± 40 mA
Maximum switching frequency, f_{sw_max}	67 kHz
Rated power	57 W
System stand-by power (estimated)	< 10 W
Ambient temperature range	– 40°C–50°C

In ICS stand-by mode and loads less than 30–35 W, this QRF operated either in the pulse-skip mode [23] or in the discontinuous-conduction mode (DCM) like a conventional flyback dc-dc converter in order to reduce losses, i.e. increase the converter efficiency. With higher loads (> 35 W), the QRF was operating in the VSM which is expected for the ICS power-transfer mode.

The control IC used was *onsemi* NCP1340 quasi-resonant multi-mode controller with valley lock-out switching feature down to 6th valley [23]. Also, additional documents [24], [25], [26] were helpful during the converter design.

The process of switch choice is the similar as for an ACF as described in [11], but here the formula is extended with an item for a short-circuit case. Hence, the rated switch voltage shall be calculated as

$$V_{DS} > 1.2 \cdot \max\left(V_{DS\_PT}, V_{DS\_SB}, V_{DS\_SC}\right) \tag{1}$$

where V_{DS_PT} and V_{DS_SB} are drain-source voltages of switch in power transfer and stand-by modes, respectively, and V_{DS_SC} is the worst-case voltage during short-circuit(s) at converter output(s). The 1.2 factor is design margin of 20%. The switch voltage in power transfer or stand-by modes (V_{DS_x}) is calculated as

$$V_{DS\_x} = V_{in\max} + n \cdot (V_{out} + V_F) \tag{2}$$

where V_{inmax} is the maximum input voltage (880 V), V_{out} regulated output voltage (5.5 V), and V_F forward voltage-drop of output Schottky diode (0.3 V). The influence of leakage inductance to expression (2) is neglected since it was observed that is was less than 2 V. Also, in (2) the influence of dynamic voltage change during short-circuit was not considered since one cannot calculate it precisely. Hence it is decided to perform several experiments and choose the biggest value of drain-source voltage. The worst-case drain-source voltage in short-circuit one gets when QRF output is shorted at maximum input voltage and minimum load that ensures VSM operation, i.e. 32 W–38 W. See chapter IV.B for more info (Fig. 16 and Fig. 17). When everything was

TABLE 2. Specification of transformer.

Parameter	Value
Maximum peak primary working voltage	> 960 V
Turns ratio primary to output 1 and 2	15
Turns ratio primary to output 3	3.75
Turns ratio primary to output 4 and 5	7.5
Core shape	ETD29
Core material	N87, TP4, DMR40…
Magnetizing inductance, L_m	600 µH
Leakage inductance, L_k	< 9 µH
Max peak primary-current, I_{pri_max}	1.82 A

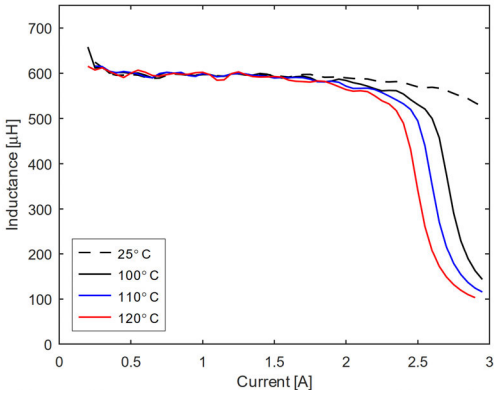

FIGURE 2. The magnetizing inductance vs. primary current and temperature of the transformer T3-3.

calculated and/or measured the expression (1) became

$$V_{DS} > 1.2 \cdot \max(976\,V, 727\,V, 1396\,V). \quad (3)$$

So based on (3) we see that one had to use 1700 V rated switch and it was the same SiC FET [27] as used in [5] and [6].

B. TRANSFORMER DATA

The design of a QRF transformer is similar to any other flyback one [4]. So, only few notes will be given here. More info on transformer design for a DCM flyback with multiple outputs is given in [28]. The specification of the transformer 60 W is listed in Table 2. It was slightly overdesigned to have some reserve power. The transformer's schematic symbol is provided in [4] and a representative photo in [8]. Note that term transformer will be used instead of the more appropriate "coupled-inductors", for a flyback converter, since it is widely used in daily engineering practice. The transformers were designed and built by four vendors per data from the Table 2. The safety distances (clearance and creepage) were calculated per [29]. In Table 3 a summary of used transformers is shown.

The measured characteristics of "magnetizing inductance vs. primary current" ($L_m(I)$) at different ambient temperatures are shown in Fig. 2 and Fig. 3. In Fig. 4 comparisons for temperatures up to 100°C are given since, in ICS, we do not expect higher temperatures than 85°C because transformer is attached to the metal housing for better cooling. The experiments presented in this paper are done with transformers T3-3 and T3-4 hence only their characteristics are presented. For those measurements the Power Choke Tester [30] and a thermal chamber were used. Regarding construction of the transformer, vendors had freedom to choose air-gap value, type of wires, and arrangement of windings. In addition, maximum peak current is 1.82 A (Table 2), which is represented in Fig. 4. From Fig. 2, Fig. 3, and Fig. 4 one can clearly see that T3-3 construction was much superior to the T3-4 one. Therefore it will be used in mass production. In Fig. 3 we can see that after 100°C the T3-4 loses magnetizing inductance significantly and one may (wrongly) think that this is another design. Hence the designer has to be aware of those effects too during detailed evaluation of the custom-made transformers and choice of vendors.

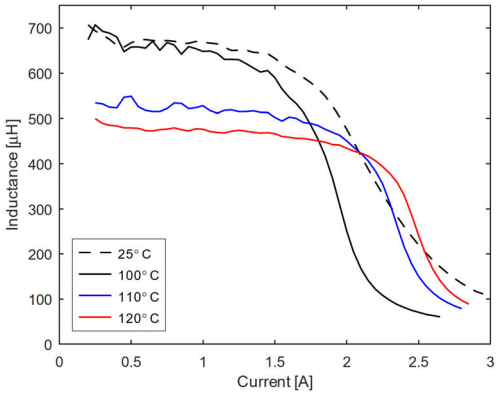

FIGURE 3. The magnetizing inductance vs. primary current and temperature of the transformer T3-4.

TABLE 3. Overview of the used transformers.

Transformer: L_m, vendor, revision
T3-1: 600 µH, vendor 1, rev. 1
T3-2: 600 µH, vendor 2
T3-3: 600 µH, vendor 3
T3-4: 600 µH, vendor 1, rev. 2
T3-5: 600 µH, vendor 4

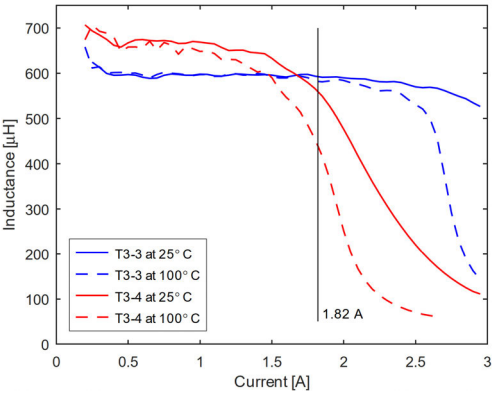

FIGURE 4. The "magnetizing inductance vs. primary current" comparison of T3-3 and T3-4 up to 100°C.

C. ABNORMAL OPERATION

In this section we will briefly discuss three modes of work which can be considered as an abnormal operation of a converter. They are start-up procedure, short-circuit, and over-power condition.

1) START-UP PROCEDURE

The detailed description of the NCP1340 start-up procedure is given in [23] and will not be repeated here in detail. The NCP1340 has soft-start function with typical duration of 4 ms—which was appropriate for this application.

In addition, the NCP1340 has integrated HV start-up circuit of 700 V [23], but that was not enough for the ICS application. In normal operation of ICS one can have dc link voltage up to 900 V—with ripple and short transients. Hence, a solution with voltage follower [31] is implemented which scales input (dc link) voltage down to 2/3 of the initial value. That allowed NCP1340 to work safely with dc link voltages up to 1050 V. Note that the schematic of voltage follower is exactly as shown in [31] so it will not be repeated here. However, during experiments an interesting phenomenon was discovered during start-up phase that will be covered in detail in section IV-B.

2) SHORT-CIRCUIT PROTECTION

The over-current protection is mandatory for any power converter. Helpful literature on understanding it with flyback converters is [32], [33], [34], and [35]. The NCP1340 is a peak-current controller and incorporates state-of-the-art solution for short-circuit protection (SCP) (see *Figure 7* in [23]). Its current limit threshold-voltage is 0.8 V, and abnormal current fault-threshold (i.e. SCP) is 1.2 V [23]. Generally, the peak-current control is often used in power supplies since it has inherent feed-forward, simplified control loop, and easy power limit [35].

The short-circuit current can be calculated in general for any converter as [11]

$$I_{SC} = I_{pri\_\max} + \frac{V_{in\max}}{L_m} \cdot t_{delay} \tag{4}$$

where I_{pri_max} is the maximum primary current (Table 2), and t_{delay} is total propagation time within the controller (350 ns [23]) and external driver (if any). The second item in (4) shall not be neglected [11]. The experimental evaluation of QRF short-circuit behavior is provided in section IV-B.

3) OVER-POWER PROTECTION

The QRF had to operate from rectified grid (single- or three-phase, and split-phase) and variable dc link voltage. It is known, from mains powered flyback designs, that at high line the maximum power capability can be much higher than desired [23], [36]. A way of limiting output power when flyback converter exhibits wide peak-current variation, depending on the input-voltage change, is named over-power protection (OPP) [25]. A general considerations for OPP of a flyback converter are provided in [36].

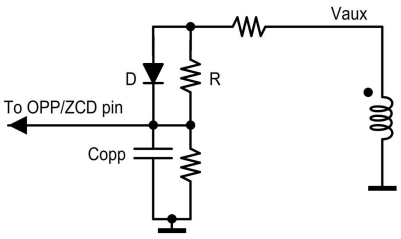

FIGURE 5. The schematic of the ZCD/OPP circuit.

In Fig. 5 [4] a solution to OPP is presented [25]—which is implemented in our QRF design. Also, that circuit is used for the zero-crossing detection (ZCD)—which is needed for correct work of a QRF with VSM. In [4] this topic was covered initially and here it is expanded. Since the NCP1340 achieves OPP without HV sensing this method is practically a non-dissipative one [23].

One can find the peak-current at high input voltage as [25]

$$I_{pkh} = \frac{0.8\,V}{R_S} + V_{in\_\max} \cdot \frac{350\,ns}{L_m} \tag{5}$$

where 0.8 V is the current-limit threshold voltage [23], R_s is the shunt resistance, V_{in_max} is highest regulated input voltage (850 V), and 350 ns is the total propagation-delay of the NCP1340 [23]. The switching period at high input voltage we get from [25]

$$T_{swh} = I_{pkh} \cdot L_m \cdot \left(\frac{1}{V_{in\_\max}} + \frac{1}{n \cdot (V_{out} + V_F)}\right) + \pi \cdot \sqrt{L_m \cdot C_{lump}} \tag{6}$$

where V_F is the forward-voltage drop of output diode, and C_{lump} is the lumped parasitic capacitance at the SN (165 pF). The high output power can be calculated as [25]

$$P_{out\_high} = 0.5 \cdot L_m \cdot I_{pkh}^2 \cdot f_{swh} \cdot \eta \tag{7}$$

where: f_{swh} is the switching-frequency at high input-voltage ($f_{swh} = 1/T_{swh}$) and η is efficiency. At the end, for this QRF one would get peak-current of 2.46 A, and maximum power of 78.76 W—which is dangerous. Hence, maximum output power in our case was limited to 60.5 W by choosing resistor R to be 1 MΩ. The calculated OPP threshold was 180 mV which gives us limited peak current of 1.92 A. If we look at the Fig. 4 then we conclude that this is not a problem for the chosen transformer T3-3.

Key-components in schematic from Fig. 5 are diode D and capacitor C_{OPP}. The role of diode is to separate OPP and ZCD actions depending on the V_{aux} polarity. It shall be rated for minimum 350 V, have low forward-voltage drop, and to be ultra-fast recovery type [4]. Otherwise, its leakage current will influence OPP detection thresholds and could cause OPP premature action. And that would force the QRF to restart.

The C_{OPP} is a filtering capacitor on ZCD/OPP pin. But it has influence on valley-detection by adding delays—depending on its value. Hence it influences the switching frequency change and valley lock-out too. Too low C_{OPP}

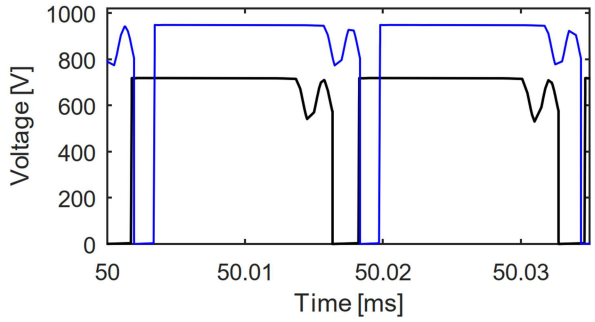

FIGURE 6. The simulated drain-source voltages in steady-state at 620 V (black) and 850 V (blue) inputs and rated load.

might cause problems during power up of the ICS. The reason is that the input dc voltage may go too much into negative (< -0.3 V) thus it may cause control IC to enter into undefined operation [23]. In our case that was auto-restart operation. More on this problem we will discuss in the experimental section. On the other side, too high C_{OPP} will cause unnecessary delays and affect change of frequency. So, one shall try to find a balance by doing several experiments. Also, noise influence can be minimized by improving the layout around control IC.

III. SIMULATION RESULTS

The QRF converter was simulated in *SIMPLIS* [37]. The total parasitic capacitance of the SN was estimated as 165 pF. Maximum switching-frequency was limited to 67 kHz. The leakage inductance (8 μH) was not included in the QRF model since it caused huge non-plausible ringing of the switch drain-voltage and increased the simulation-time a lot. Here we will cover only operation in ICS power transfer mode for sake of the paper completeness. The results for QRF when ICS was in stand-by mode are given in [4].

The simulation results of drain-source voltage, primary current, and voltage of zero-crossing detection (ZCD) pin at 620 V and 850 V inputs and 57 W load are shown in Fig. 6, Fig. 7, and Fig. 8. The QRF was working in VSM. There one can notice that the valley-switching is working as expected and switch turn-on happens at second valley for both input voltages. The clamped-voltages of switch Q (i.e. SN point) by RCD snubber were 719 V and 949 V. The QRF model was somewhat idealized hence high-frequency voltage ringing at switch turn-off is not visible in Fig. 6. The switching frequencies were 59.6 kHz and 59.21 kHz, at 620 V and 850 V, respectively. The primary currents are presented in Fig. 7 with peak values of 2.04 A and 2.08 A at 620 V and 850 V inputs, respectively. From Fig. 8 we read minimum voltages on ZCD/OPP pin as -125 mV and -170 mV at 620 V and 850 V inputs, respectively. And this is good since it is less, in absolute terms, than the calculated OPP limit of -180 mV.

IV. EXPERIMENTAL RESULTS AND DISCUSSION

The QRF converter, as specified in Table 1, was built and tested. The photo of the implementation in ICS is given in Fig. 9. But all tests were actually done on a prototype board

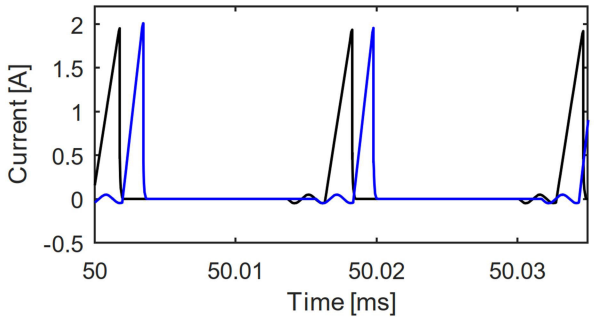

FIGURE 7. The simulated primary currents in steady-state at 620 V (black) and 850 V (blue) inputs and rated load.

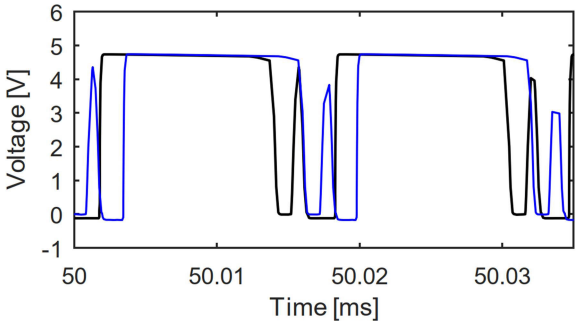

FIGURE 8. The simulated ZCD voltages in steady-state at 620 V (black) and 850 V (blue) inputs and rated load.

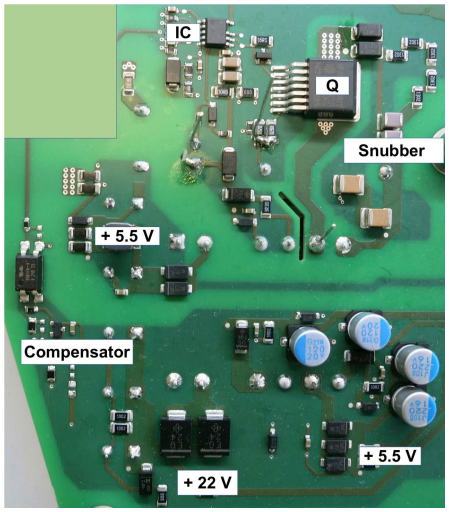

FIGURE 9. Photo of the 57 W QRF in ICS (top-view).

in a way that both 5.5 V and 22 V outputs were loaded by dc-electronic-loads whilst the $\pm$11 V outputs had only bleeder resistors of 10 kΩ as small loads [5]. This was done to make testing easier and had no influence on the conclusions.

A. OPERATION IN ICS POWER-TRANSFER MODE

The same waveforms, as in simulation section, at 620 V and 850 V input voltages and 57 W loads are presented in Fig. 10, Fig. 11, and Fig. 12. There one can see that resulting waveforms are well matched with the measured ones.

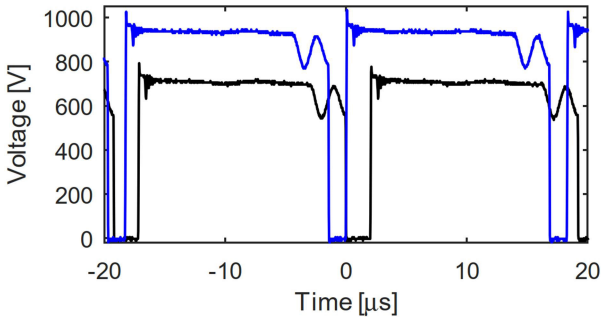

FIGURE 10. The measured drain-source voltages in steady-state at 620 V (black) and 850 V (blue) inputs and rated load.

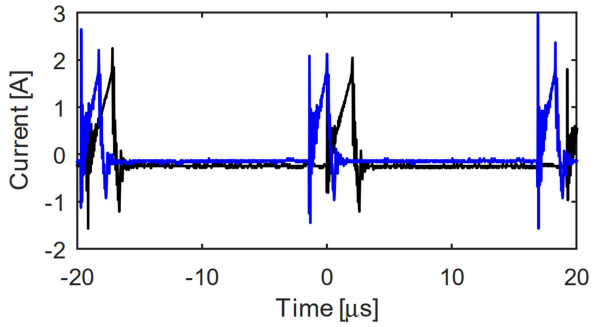

FIGURE 11. The measured primary currents in steady-state at 620 V (black) and 850 V (blue) inputs and rated load.

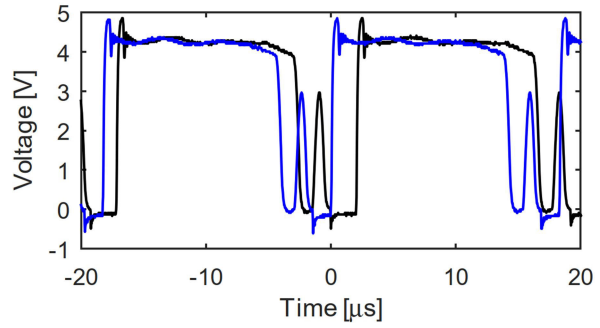

FIGURE 12. The measured ZCD voltages in steady-state at 620 V (black) and 850 V (blue) inputs and rated load.

From Fig. 10 we see that the valley-switching is working as expected and switch turn-on happens at second valley for both input voltages like in simulations. Note that experimental waveforms are taken for C_{OPP} of 100 pF.

One can see that the (RCD clamped) drain-source voltages are a bit lower than in simulations (Fig. 6). And that is good because it is on a side of safety. Also, we can wee that the maximum currents (ringing excluded) are lower than the simulated ones—which is good—and they are matched with the calculated one from Table 2. The ZCD voltages in Fig. 12 are well matched with the simulated ones in Fig. 8.

B. ABNORMAL OPERATIONS

In this section we will analyze two cases of abnormal operation that happened in practice during QRF testing.

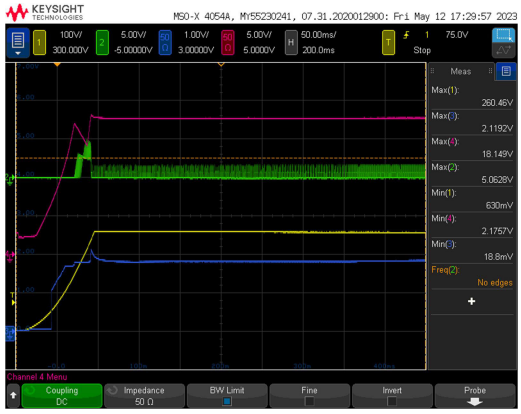

FIGURE 13. The QRF normal startup sequence from dc input.

1) START-UP PROBLEM

The QRF was working as expected when supplied directly from a dc source either on a demo board or in the system. And the key-waveforms during normal start-up of QRF are shown in Fig. 13. There we can see that fault-pin is around 1.78 V and that is within non-fault range of NCP1340 [23]. In Fig. 13. and Fig. 14 the following legend is valid: **CH1** (yellow; 100 V/div; dc link voltage), **CH2** (green; 5 V/div; gate-source voltage), **CH3** (blue; 1 V/div; fault-pin voltage of NCP1340, and **CH4** (red; 5 V/div; Vdd voltage of NCP1340).

Sometimes, when powered from mains, in a system, the QRF would enter auto-recovery operation with fault pin [23] pulled to ground (see Fig. 14). This effect was not happening on every board, where QRF was implemented, i.e. it was random. The probable reason was too negative voltage (less than $-$ 0.3 V) on ZCD pin, at power up, as a consequence of ringing in dc link (Fig. 15). And that was depending on layout tolerances and instant when mains voltage was turned on. The dc link voltage change was result of mains-voltage rectification by body diodes in PFC (power-factor corrector) stage. The solution was to increase C_{OPP} to 100 pF. In Fig. 12 one can see that the ZCD voltage has negative spike—which was not critical. But it was probably amplified during power-up from the grid when dc link shortly goes into negative down to -9 V (Fig. 15). Hence, increasing C_{OPP} helped in filtering on this pin thus avoiding disturbance of the QRF operation. However, this change affected valley lock-out and switching frequency so efficiency and Bode plots had to be measured again. Those results will be discussed in following sections.

2) SHORT-CIRCUIT TESTS

Protection against short-circuit is an important aspect of design of a dc-dc converter. The QRF and its controller NCP1340 [23] are not an exception and, since it is a peak-current controller, it is easy to achieve current limitation. The evaluation of short-circuits at QRF outputs was done in similar manner as for the ACF converter in [5], but more test-cases were considered here. Hence, this is the most comprehensive practical evaluation of short-circuit operation of a flyback converter with multiple outputs so far. During experiments

FIGURE 14. The QRF in system not starting when supplied from rectified mains.

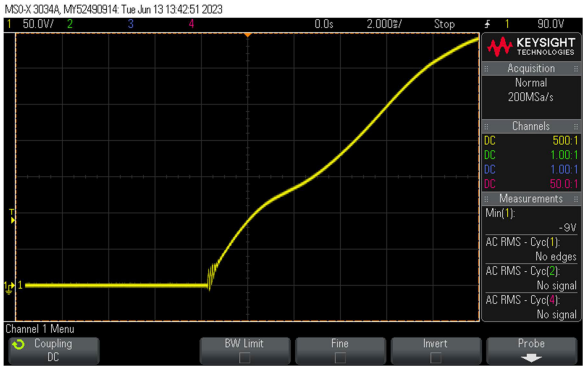

FIGURE 15. The dc link voltage rise when mains supply is turnedon.

the peak primary current, input power and temperature of semiconductors were observed.

Creation of short-circuits at QRF converter's outputs during operation was done by dc electronic load [38] which had such a (useful) feature. The usage of 1–0 or rocker switches was not good since one could observe bouncing of their contacts; hence results were not so plausible. Following tests were executed and evaluated:

1) Start-up when regulated output 5.5 V is shorted;
2) Regulated output 5.5 V shorted during operation in pulse-skip mode (= no load);
3) Regulated output 5.5 V shorted during operation in VSM at 650 V and 850 V inputs (see Fig. 16);
4) Start-up when non-regulated output 5.5 V is shorted;
5) Non-regulated output 5.5 V shorted during operation in pulse-skip mode (= no load) (see Fig. 18);
6) Non-regulated output 5.5 V shorted during operation in VSM at 650 V and 850 V inputs;
7) Start-up when non-regulated output 22 V is shorted;
8) Non-regulated output 22 V shorted during operation in pulse-skip mode (= no load);
9) Non-regulated output 22 V shorted during operation in VSM at 650 V and 850 V inputs (see Fig. 17).

The shorts at ± 11 V non-regulated outputs were not analyzed since they are designed for very small load and it was not easy to make short-circuits at those terminals as well. But one

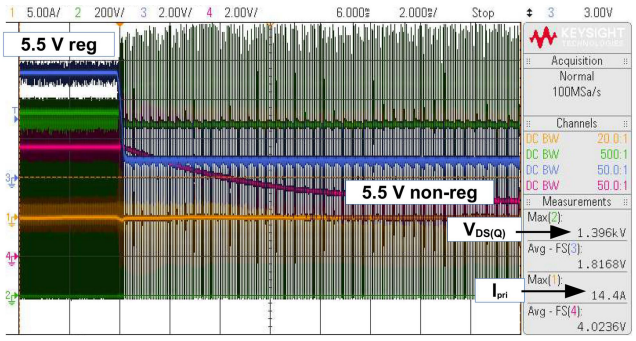

FIGURE 16. The 5.5 V regulated output shorted (blue). QRF in VSM (6^{th} valley) at 850 V input.

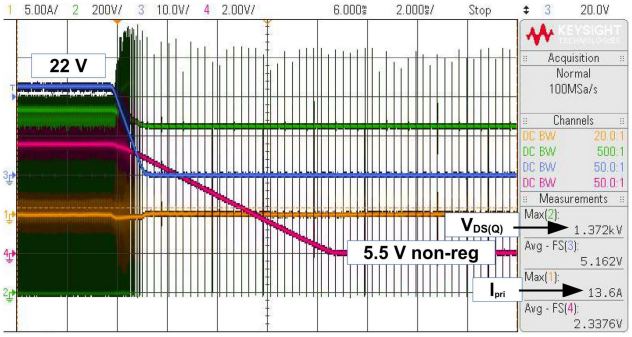

FIGURE 17. The 22 V non-regulated output shorted (blue). QRF in VSM (6^{th} valley) at 850 V input.

can assume that the behavior would be similar as for the non-regulated 5.5 V output.

The short-circuits at QRF outputs, when converter was operating in VSM, were detected and peak current was limited as expected and QRF would turn-off (see Fig. 16 and Fig. 17). However, shorting non-regulated outputs 5.5 V or 22 V in pulse-skip mode, i.e. no load, resulted in undetected short-circuits. Moreover, in a case when non-regulated 5.5 V output was shorted, the regulated one was still properly regulated to 5.5 V like that nothing happened (see Fig. 18). Similar effect was observed as well when QRF was starting and non-regulated 5.5 V output was already shorted. The maximum measured rms output currents when converter outputs were shorted at 640 V dc input and no load (pulse-skip mode) were: 3.66 A (5.5 V regulated output shorted), 7.07 A (5.5 V non-regulated output shorted), and 4.81 A (22 V non-regulated output shorted). The maximum measured input power was 12.3 W in a condition when the 5.5 V non-regulated output was shorted. Note that during short-circuits one could hear audible noise as well.

The cases with undetected short-circuits are undesirable for a converter that is employed in field. Hence, following mitigation strategies have to be considered during converter design:

- Usage of control IC that has latched behavior during such faults, i.e. auto-restart mode is not desirable;
- Diodes at converter outputs have to be able to withstand permanent short-circuit condition;

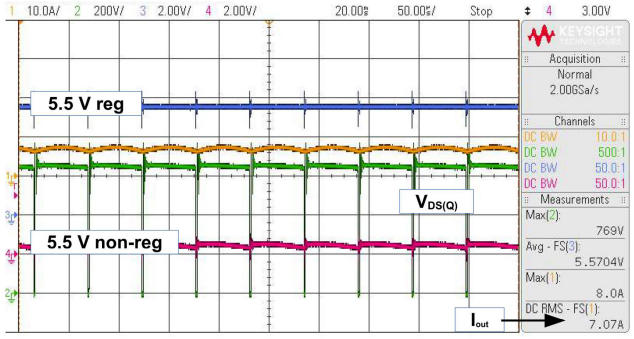

FIGURE 18. The 5.5 V non-regulated output shorted (red). QRF in pulse-skip mode at 640 V input and no load.

- Optional: Voltage monitoring circuits have to be used which can turn-off the controller. However, this will increase price and complexity of the converter;
- Fuses shall be added at converter outputs;
- Optional: vendors of control ICs to consider such situation in future developments and implement some new measures (if possible).

Main criteria when choosing mitigation strategy are to avoid that transformer catches a fire, i.e. windings burn, and/or some components explode. Overdesigning the transformer is often techno-economically not feasible due to space and price constraints. Hence it is not mentioned in the above list. The short-circuit testing is normal part of the certification process. Note that in our case evaluation of short-circuits shall be done according to standards [39], [40], [41].

C. EFFICIENCY AND LOSSES MEASUREMENTS

The QRF efficiency measurements are provided in Fig. 19 for the T3-3 (with C_{OPP} of 56 pF) and T3-4 (with C_{OPP} of 100 pF) transformers. The self-consumption of the primary side was estimated and considered in efficiency calculations. As expected, the efficiency at lower input voltage is higher due to lower switching losses. In Fig. 19 the maximum efficiencies of 87.1% at 620 V and 85.1% at 850 V inputs were achieved with the T3-3. From Fig. 24 we see that, although with C_{OPP} of 100 pF the switching frequency was lower, and we expected to get increased efficiency, that could not compensate the higher other types of losses with transformer T3-4. Please note that in [4] the T3-3 was mistakenly referred as T3-1.

In Fig. 20 the efficiency of QRF with T3-4 transformer with C_{OPP} of 100 pF is analyzed when load was increasing (*up*) and decreasing (*down*). Hence influence of hysteresis in VSM operation was considered. We know that depending on load direction change the switching frequency will change differently [23]. Hence that will be reflected in the QRF converter efficiency as well. From Fig. 20 we see that this effect has bigger impact when load is less than 35 W and that is the area where QRF operates in DCM. Therefore, when presenting efficiency graphs of converters with variable switching frequency and hysteresis, it shall be stated whether load was decreasing or increasing during such experiments.

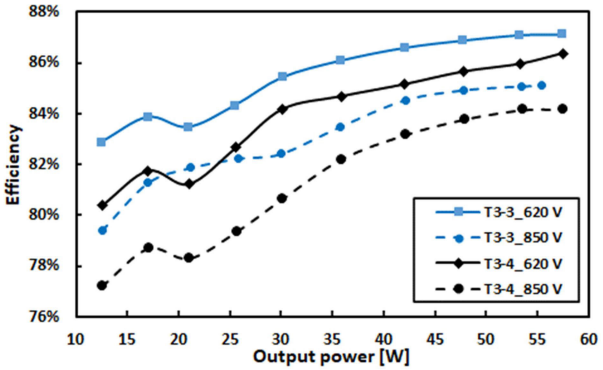

FIGURE 19. The QRF efficiency with T3-3 and T3-4.

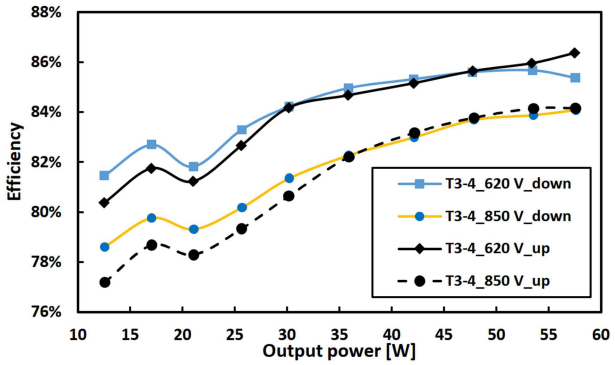

FIGURE 20. The QRF efficiency differences when load is increasing (*up*) and decreasing (*down*).

Note that in Fig. 19 loads were increasing for graphs at 620 V inputs, but decreasing for graphs at 850 V inputs. The reasons for such approach were simple: that was easier to do and would show us max/min efficiency range.

The Fig. 21 shows measured QRF "*power losses vs. input voltage*" for transformers T3-3 and T3-4. And we can see that no-load losses with T3-4 were lower. Those graphs were created out of measured input-power consumption, without load, then subtracting self-consumption and loads on bleeder resistors. We see that the converter losses themselves were predominant. In addition, a trend-line is added to the graph showing weak quadratic dependency of QRF power losses vs. input voltage. If we compare those results with the ones for ACF converter in [5] (see *Figure 18* and *Figure 19* there) then we can see how big difference is. This is due to absence of circulation energy—which is present in ACF. Note that no-load losses were not key design criteria. The Fig. 21 served following purposes: to show that those losses cannot be very low (e.g. max 250 mW), that they increase with increase of input voltage, and for comparison of different transformer constructions.

D. THERMAL MEASUREMENTS

Two kind of thermal tests were done. First, the thermal test was done on a demo-board at room temperature of approx. 25°C and is shown in Fig. 22. In Fig. 22 only 850 V results are shown because they are more severe. There we see that the power switch Q has maximum temperature of 85.4°C.

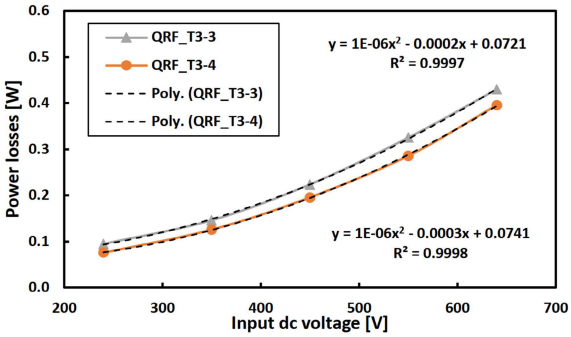

FIGURE 21. The QRF power losses vs. input dc voltage. Black dashed lines: Microsoft®. Excel® polynomial trend-lines with related expressions.

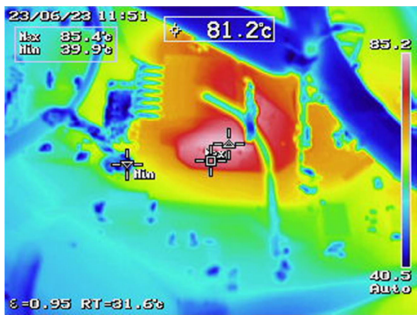

FIGURE 22. The QRF thermal test with T3-4.

The snubber diode had temperature close to the Q and it was expected that both parts will be the hottest ones. This result was acceptable. In other, non-documented measurements, it was noticed that temperatures of both were ≤86°C. Note that this experiment was done with increased gate-resistor (R_{gate}) to 100 Ω—which was consequence of EMI investigations. When compared with results in [4] (with R_{gate} of 16 Ω) we see that increase of R_{gate} contributed to around 6°C increase of switch temperature—which is acceptable. Hence, cooling of any part was not needed.

That was verified in the ICS with more than two hours test (Fig. 23) at 25°C ambient and old R_{gate} of 16 Ω. In Fig. 23 we can see that those results were good. If one would add 25°C on those results, to incorporate allowed increase of ambient temperature to 50°C, and 6°C increase for switch with R_{gate} of 100 Ω, then we will still be in the safe area. Moreover, the Fig. 23 also tells us that QRF does not work at rated power of 57 W, as designed, but less. In addition, the QRF was shortly tested at – 40°C and 50°C ambient temperatures without any problems. Note that on a bench test the T3-4 was used—which was thermally worse case since its losses are higher (see Fig. 19). But that part will not be used in series production so ICS test is done with part T3-3 (Fig. 23). In both experiments the C_{OPP} was 100 pF. As a conclusion, one can say the overall QRF thermal performance was satisfying.

E. PRACTICAL CONTROL ASPECTS

The used compensator was ATL431 [42] based Type-2 (integrator, dc gain, pole and zero) one with an opto-coupler.

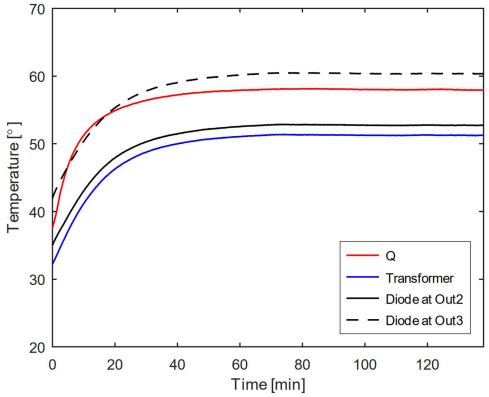

FIGURE 23. Long-term thermal test of the QRF in ICS in power-transfer mode with T3-3.

A detailed analysis of QRF control is presented in [4] hence will not be repeated here. Our focus here will be on switching frequency change, transition thresholds between DCM and VSM, and C_{OPP} influence on Bode plots.

1) SWITCHING FREQUENCY CHANGE

The measured "switching-frequency vs. load" curve is shown in Fig. 24. The maximum switching frequency was limited to 67 kHz because, in this application, there were no benefits with higher ones [4]. In Fig. 24, at different loads and input voltages, the switching frequency was changing in the range from 37.4 kHz to 54.8 kHz.

Additionally, in Fig. 24 switching-frequency change of T3-3 from [4] was included for comparison. There one can clearly see that increased C_{OPP} (from 56 pF to 100 pF) reduced the switching frequency for approx. 6 kHz for both input voltages. But if we look at efficiency comparison in Fig. 19, we can see that, despite reduced switching frequency, losses with T3-4 (and C_{OPP} of 100 pF) were much higher than the ones with T3-3 (and C_{OPP} of 56 pF). This gives us hint that, when choosing custom-made transformers, one needs to do such detailed evaluation and testing.

2) TRANSITION THRESHOLDS TO VALLEY-SWITCHING MODE

While doing experiments it was noticed that transition thresholds between DCM and VSM vary with input voltage, load, and that they depend on the chosen regulated output [4]. It was possible to identify input powers at which those transitions happen. The transition thresholds were determined by slowly increasing load simultaneously at three major outputs, and observing drain-source waveforms on the oscilloscope. In those experiments the QRF load was always increasing for all input voltages, i.e., hysteresis effect was not considered [4].

The resulting graph is shown in Fig. 25. In Fig. 25 the QRF operated in VSM starting from the 6th valley—independent on the regulated output or input voltage. And that was expected as stated in [23]. One can see that, if regulation happens at output with higher load (i.e., Output 2;

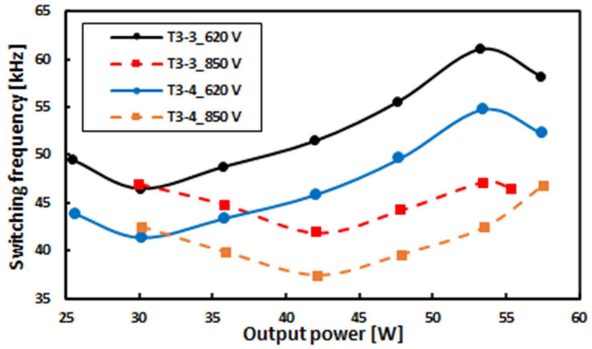

FIGURE 24. The 57 W QRF switching frequency change for two different transformers and C_{OPP}.

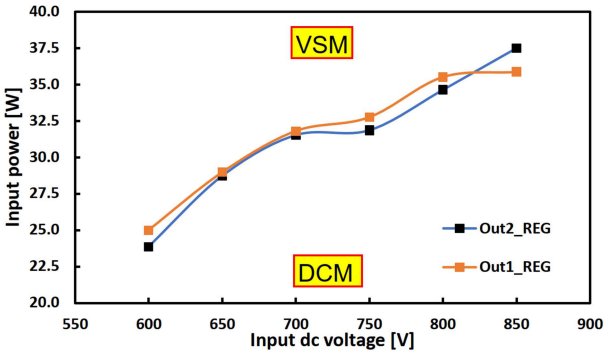

FIGURE 25. QRF transition thresholds from DCM to the valley-switching mode.

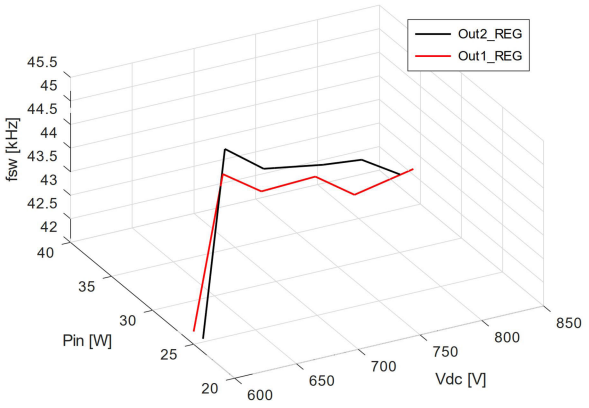

FIGURE 26. The switching-frequency change related to QRF transition thresholds from Fig. 25.

FIGURE 27. The unwanted QRF behaviour, mixed DCM and pulse-skip mode, at 850 V and 16 W input power.

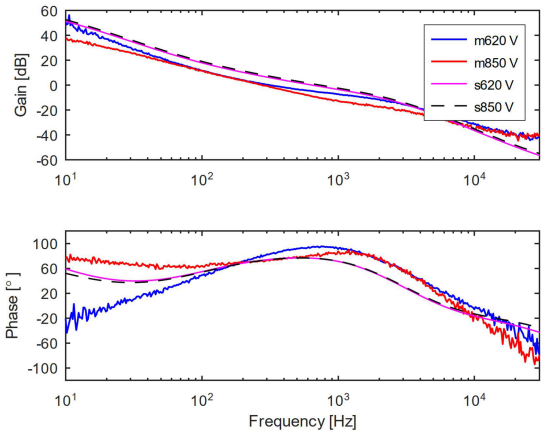

FIGURE 28. Measured (m) Bode plots with C_{OPP} 100 pF and simulated (s) ones at 620 V and 850 V.

*Out2_REG*in Fig. 25) then the QRF earlier enters the VSM—except at 850 V point. And this is desirable. When compared to the results in [4] (*Figure 43*) we see that, with increased resolution of input voltages, i.e. increased number of considered voltages, we do not see linear dependence of those thresholds vs. input voltage anymore. The reason was simply that in [4] only two measurement points were considered (620 V and 850 V) so it was possible to draw only a straight line. The small difference to results from [4] is that now gate resistor is a bit higher (100 Ω vs. 16 Ω) and C_{OPP} was higher as well (100 pF vs. 56 pF). Also, one can see that influence of the regulated output was no not so big like in [4]. So, results in Fig. 25 are more accurate and plausible, and gave us better insight into this problematic.

The Fig. 26 shows switching-frequency change related to results in Fig. 25. There we can see that range of change is not so big (from 42.3 kHz to 45.3 kHz).

Interesting phenomenon was observed at 850 V when load was less than 20 W. There the QRF was operating in a kind of transition between DCM and pulse-skip modes (see Fig. 27). Such unwanted behaviour was unavoidable and it is inherent to how NCP1340 works and decides on valley and mode change [23], [43], [44]. And one could not do anything about it. In Fig. 27 the following legend is valid: **CH2** (green; 200 V/div; drain-source voltage), **CH3** (blue; 5 V/div; gate-source voltage, and **CH4** (red; 0.5 V/div; feedback voltage of the NCP1340).

3) BODE PLOTS

The Bode plots of QRF operating in VSM were measured with Bode 100 vector network-analyzer [45] and excitation signal was 50 mV (peak-to-peak). The regulated 5.5 V output was the Output 2 (Table 2). All Bode plots had first-order

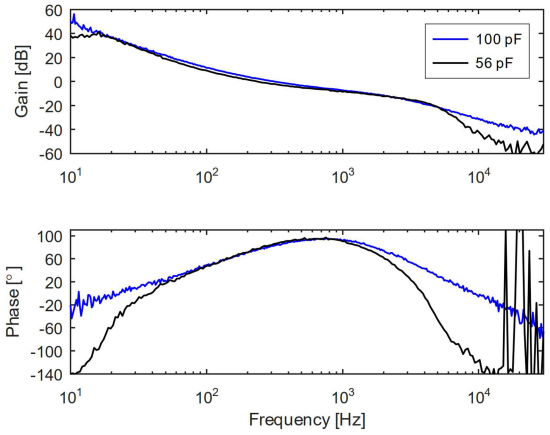

FIGURE 29. Bode plots at 620 V with C_{OPP} 100 pF vs. 56 pF.

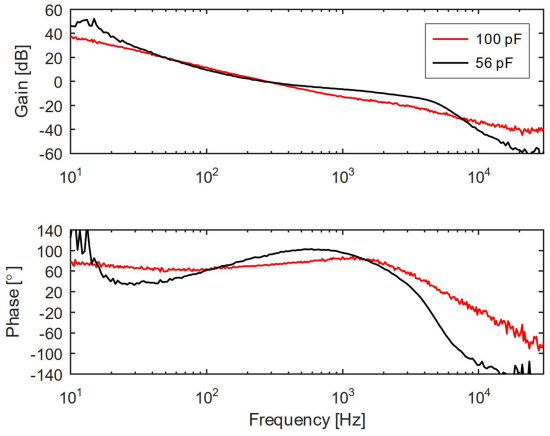

FIGURE 30. Bode plots at 850 V with C_{OPP} 100 pF vs. 56 pF.

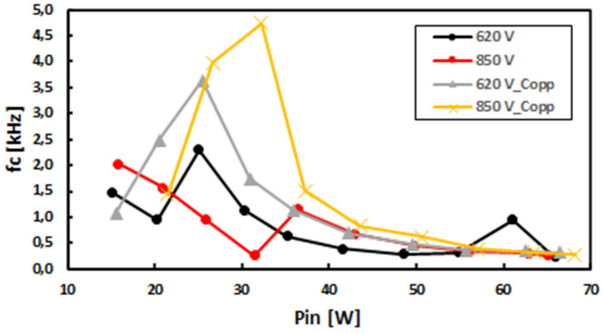

FIGURE 31. The QRF converter: bandwidth change with input voltage, input power, and C_{OPP} =100 pF.

response (Fig. 28)—which is typical for any peak-current controlled flyback dc-dc converter [46].

In Fig. 28 measured (m) results at rated power and 620 V vs. 850 V voltages are analysed. Also, in Fig. 28 simulated (s) Bode plots are shown. The simulation model is made by modification of generic QRF model from [47] (*page 584*). From [4] (*Figure 14*) and Fig. 28 we see that when using such generic simulation model for QRF there is not big difference on simulated Bode plots at 620 V and 850 V. Moreover, since C_{OPP} was not part of the generic simulation model one could

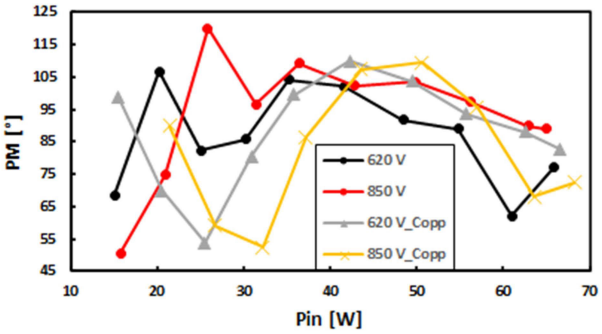

FIGURE 32. The QRF converter: phase-margin change with input voltage, input power, and C_{OPP} =100 pF.

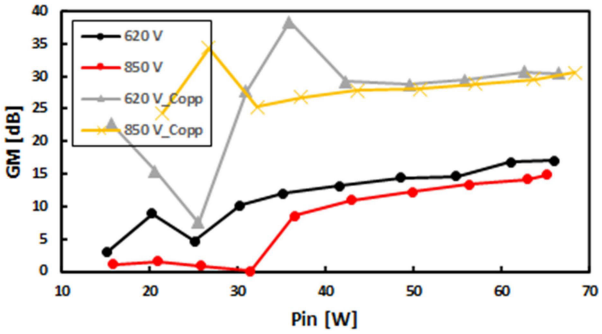

FIGURE 33. The QRF converter: gain-margin change with input voltage, input power, and C_{OPP} =100 pF.

not see its influence. In Fig. 29 and Fig. 30 the comparisons of measured Bode plots, with different C_{OPP} and input voltages of 620 V and 850 V, respectively, are provided. There one can see that with C_{OPP} of 100 pF one had much better responses. The detailed theoretical and mathematical analysis might be part of a future study.

The changes of bandwidth (cross-over frequency; fc), phase-margin (PM), and gain-margin (GM) in whole load-range are shown in Fig. 31–Fig. 33. This follows our strategy which was presented in [4]. From measured Bode plots, for every operating point, the fc, PM, and GM were extracted. Those quantities were plotted vs. input power because that was much faster and easier to do. Operation at 10 loads and two input voltages were considered.

In Fig. 31–Fig. 33 comparison to the graphs from [4] (with C_{OPP} of 56 pF; not marked on graphs) are presented so that one can analyse influence of C_{OPP} increase to 100 pF value (marked as "_C_{OPP}" on graphs). It is evident that all measured quantities are higher than those in the original design [4]. Also, one can see that all three quantities are changeable with load and input voltage—as expected. From practical experience, the PM shall be >40° and GM>6 dB for all operating conditions [4]. We see that those are fulfilled everywhere. Moreover, the bandwidth was in 0.28–4.73 kHz range—which was acceptable. Conclusion is that no stability problems are expected since new results are much better than the original ones from [4] and in ICS normal operation the input power of QRF is always higher than 35 W.

V. SUMMARY AND CONCLUSION

The paper presented practical investigation of QRF with VSM dc-dc converter 57 W used as APS of the primary side of an ICS for battery electric vehicles. In [4] was shown that QRF is better topology for this emerging application when compared to ACF (active-clamped flyback) converter, except for EMI. In addition, in [4] more design-related data are revealed so they were not repeated here. Anyway, analysis presented here and in [4] demonstrated that QRF with VSM is appropriate topology for this emerging application although it has two small shortcomings presented below.

The findings and conclusions presented here are valid for any QRF converter (e.g. start-up problem, OPP, control); and some are valid for any flyback or other isolated dc-dc converters (e.g. short-circuits, transition thresholds with multi-mode converters, evaluation of transformers, load direction-change influence on converter efficiency when switching frequency is variable).

The comprehensive analysis of abnormal operations (i.e. start-up, short-circuit and over-power) was presented for the first time and is applicable to other types of flyback converters too. Also, the additional control aspects, when compared to [4], were covered as well. One could see that a solution to unwanted effect of converter, not being able to start under some conditions, positively influenced switching-frequency change, efficiency, and Bode plots, i.e. control loop response. The solution was simply to increase filtering capacitor on ZCD/OPP control pin.

Thermal behavior of transformer and QRF were investigated on a demo-board and in a system for a longer time. And results were satisfying without need for any additional measures.

Evaluation of short-circuits at converter outputs was done through nine test-cases and is most comprehensive overview of short-circuits with flyback converters so far. When QRF operated in VSM the short-circuit protection worked as expected. But, if short-circuit happens at non-regulated output, at no load, it may go undetected. And this is the main shortcoming of this converter in this application. Hence, several mitigation strategies were proposed with goal of preventing that transformer burns or some other parts explode.

Limitations of this study are following:

- There was no freedom in choice of the control method since commercial control IC was used. Moreover, at some light load unwanted transitions between DCM and pulse-skip modes is discovered, but one was not able to do anything about it except ensuring that converter has enough load above the critical one. And this is the second shortcoming of this converter in this application.
- This work is part of a running commercial project so not all design data could have been revealed.
- Some formulas are created by curve-fitting of the experimental curves.
- There was no focus of mathematical modeling.

The future work might be on mathematical modeling of C_{OPP} influence on small-signal model or modeling of transition thresholds, and on EMI aspects (e.g. conducted emissions).

DECLARATION

Author declares no conflict of interests that could have influenced the work reported in this paper and do not endorse any manufacturer of electronic components or test equipment. No text was generated by using artificial intelligence (AI).

ACKNOWLEDGMENT

The author would like to thank United Silicon Carbide Inc. for providing samples of the SiC FETs, transformers' suppliers, and Christophe Basso for tips during troubleshooting of the QRF start-up problem. Support from management of BRUSA, especially L. Böhler; engineers R. Raval, A. Ramos, A. R. Nallamaddireddy, and ex-colleagues A. Diefenthaler and N. Vias is appreciated.

Some of the figures were made or edited by using *FidoCADJ* [48], *GNU Octave* [49], and *Libre Office Draw* [50]. The references were managed in Zotero [51].

REFERENCES

[1] IEA (Apr. 2023). *The Global EV Outlook 2023*. IEA, Paris, France. Accessed: Aug. 1, 2023. [Online]. Available: https://www.iea.org/reports/global-ev-outlook-2023

[2] Shell Recharge Solutions. (May 2023). *EV Driver Survey report 2023*. Shell Recharge Solutions. Accessed: Aug. 19, 2023. [Online]. Available: https://shellrecharge.com/en-gb/solutions/knowledge-centre/reports-and-case-studies/ev-driver-survey-report

[3] A. Mahesh, B. Chokkalingam, and L. Mihet-Popa, "Inductive wireless power transfer charging for electric Vehicles–A review," *IEEE Access*, vol. 9, pp. 137667–137713, 2021, doi: 10.1109/ACCESS.2021.3116678.

[4] D. Đ. Vračar, "Quasi-resonant flyback converter as auxiliary power-supply of an 800 v inductive-charging system for electric vehicles," *IEEE Access*, vol. 10, pp. 109609–109625, 2022, doi: 10.1109/ACCESS.2022.3214526.

[5] D. Đ. Vračar and P. V. PEJOVIC, "Active-clamp flyback converter as auxiliary power-supply of an 800 V inductive-charging system for electric vehicles," *IEEE Access*, vol. 10, pp. 38254–38271, 2022, doi: 10.1109/ACCESS.2022.3165059.

[6] D. Vračar and M. Pavlovsky, "Implementation of active-clamped flyback DC–DC converter in an 800 V system," in *Proc. PCIM Eur. Digit. Days, Int. Exhib. Conf. Power Electron., Intell. Motion, Renew. Energy Energy Manage.*, May 2021, pp. 1–8. [Online]. Available: https://ieeexplore.ieee.org/document/9472384

[7] D. Đ. Vračar, M. Pavlovský, and P. Pejovic, "Active-clamped flyback DC–DC converter in three-phase application," in *Proc. 21st Int. Symp. Power Electron. (Ee)*, Oct. 2021, pp. 1–6, doi: 10.1109/Ee53374.2021.9628263.

[8] D. Vračar and P. Pejović, "Active-clamped flyback DC–DC converter in an 800 V application: Design notes and control aspects," *J. Electr. Eng.*, vol. 73, no. 4, pp. 237–247, Aug. 2022, doi: 10.2478/jee-2022-0032.

[9] D. Vračar, "Active-clamped flyback converter: Dynamic load and cross-regulation aspects," in *Proc. 22nd Int. Symp. Power Electron. (Ee)*, Oct. 2023, pp. 1–6, doi: 10.1109/Ee59906.2023.10346170.

[10] D. Vračar, S. Wüstner, and A. Boulos, "Wireless inductive charging of battery electric vehicles is coming," *IEEE Power Electron. Mag.*, vol. 10, no. 3, pp. 36–42, Sep. 2023, doi: 10.1109/MPEL.2023.3301428.

[11] D. Vračar, "Modern solution of inductive charging system for 800 v batteries of electric vehicles," in *Proc. 22nd Int. Symp. Power Electron. (Ee)*, Oct. 2023, pp. 1–10, doi: 10.1109/Ee59906.2023.10346167.

[12] Y. Panov and M. M. Jovanovic, "Adaptive off-time control for variable-frequency, soft-switched flyback converter at light loads," in *Proc. 30th Annu. IEEE Power Electron. Spec. Conf. Rec.*, Jul. 1999, pp. 457–462, doi: 10.1109/PESC.1999.789046.

[13] G. Mauromicale, A. Raciti, S. A. Rizzo, G. Susinni, F. Fusillo, A. Palermo, F. Scrimizzi, and R. Scollo, "Si and GaN devices in quasi resonant flyback converters for wall charger applications," in *Proc. IEEE Energy Convers. Congr. Expo. (ECCE)*, Sep. 2019, pp. 3253–3258, doi: 10.1109/ECCE.2019.8912178.

[14] Y. Mo, H. Qin, W. Chen, Y. Yang, S. Wang, L. Hu, and L. Xie, "Auxiliary power supply with SiC MOSFET for wide-range high voltage input applications," in *Proc. IEEE 9th Int. Power Electron. Motion Control Conf. (IPEMC-ECCE Asia)*, Nov. 2020, pp. 137–141, doi: 10.1109/IPEMC-ECCEAsia48364.2020.9368165.

[15] Y. Sahin and G. Tohumoglu, "Quasi resonant flyback topology based LCD TV power supply board design and power loss analysis," in *Proc. 2nd Eur. Conf. Electr. Eng. Comput. Sci. (EECS)*. Bern, Switzerland, Dec. 2018, pp. 16–20, doi: 10.1109/EECS.2018.00012.

[16] H. Onay, V. Sueel, and A. Hava, "A comprehensive loss analysis of quasi resonant flyback converter for design purpose," in *Proc. PCIM Asia, Int. Exhib. Conf. Power Electron., Intell. Motion, Renew. Energy Energy Manage.*, Jun. 2018, pp. 1–8.

[17] Y. Panov and M. M. Jovanovic, "Adaptive off-time control for variable-frequency, soft-switched flyback converter at light loads," *IEEE Trans. Power Electron.*, vol. 17, no. 4, pp. 596–603, Jul. 2002, doi: 10.1109/TPEL.2002.800958.

[18] Y.-B. Park and H.-S. Choi, "A hybrid control method to maximize efficiency for active mode efficiency regulation," in *Proc. INTELEC 29th Int. Telecommun. Energy Conf.*, Sep. 2007, pp. 83–88, doi: 10.1109/INTLEC.2007.4448743.

[19] R. D. Stracquadaini, "Mixed mode control (fixed off time & quasi resonant) for flyback converter," in *Proc. IECON - 36th Annu. Conf. IEEE Ind. Electron. Soc.*, Nov. 2010, pp. 556–561, doi: 10.1109/IECON.2010.5675222.

[20] J. Park, Y.-J. Moon, M.-G. Jeong, J.-G. Kang, S.-H. Kim, J.-C. Gong, and C. Yoo, "Quasi-resonant (QR) controller with adaptive switching frequency reduction scheme for flyback converter," *IEEE Trans. Ind. Electron.*, vol. 63, no. 6, pp. 3571–3581, Jun. 2016, doi: 10.1109/TIE.2016.2523931.

[21] Q. Wu, X. Li, Y. Han, Z. Di, and Q. Feng, "A valley-locking control scheme for an audible noise-free Valley-Skip-Mode flyback converter," *IEEE Trans. Ind. Electron.*, vol. 69, no. 7, pp. 7285–7294, Jul. 2022, doi: 10.1109/TIE.2021.3099223.

[22] W. Langeslag, R. Pagano, K. Schetters, A. Strijker, and A. van Zoest, "A high-voltage compatible BCD SoC-ASIC performing valley-switching control of AC–DC power converters based on PFC and flyback cells," in *Proc. IECON - 32nd Annu. Conf. IEEE Ind. Electron.*, Nov. 2006, pp. 2996–3001, doi: 10.1109/IECON.2006.347505.

[23] Datasheet. (Mar. 2021). *NCP1340: Quasi-Resonant Controller, High-Voltage, Featuring Valley Lock-Out Switching*. Onsemi, Accessed: May 8, 2022. [Online]. Available: www.onsemi.com

[24] Application Note. (Jul. 2014). *Designing a Quasi-Resonant Adaptor Driven by the NCP1339*. Onsemi. Accessed: May 8, 2022. [Online]. Available: www.onsemi.com

[25] Application Note. (Dec. 2009). *Designing a Quasi-Resonant Adaptor Driven by the NCP1380*. Onsemi. Accessed: May 8, 2022. [Online]. Available: www.onsemi.com

[26] C. Adragna. (Nov. 2002). *AN1326: L6565 Quasi-Resonant Controller*. STMicroelectronics. Accessed: Jun. 6, 2022. [Online]. Available: www.st.com

[27] Datasheet. (Nov. 2022). *UF3C170400B7S, 1700 V, SiC FET*. UnitedSiC. Accessed: Sep. 3, 2023. [Online]. Available: https://www.qorvo.com/products/power-solutions/sic-fets

[28] A. Ayachit, A. Reatti, and M. K. Kazimierczuk, "Magnetising inductance of multiple-output flyback DC–DC convertor for discontinuous-conduction mode," *IET Power Electron.*, vol. 10, no. 4, pp. 451–461, Mar. 2017, doi: 10.1049/iet-pel.2016.0390.

[29] *Safety of Transformers, Reactors, Power Supply Units and Combinations There of—Part 2–16: Particular Requirements and Tests for switch Mode Power Supply Units and Transformers for Switch Mode Power Supply Units for General Applications*, document IEC 61558-2-16:2021, 2021.

[30] Description and Technical Specifications. (Jan. 2021). *Power Choke Tester DPG10B Series*. ED-K. Accessed: Apr. 15, 2022. [Online]. Available: www.ed-k.de

[31] Application Note. (Dec. 2020). *AN5548: Ultra-Wide Range 100 W Flyback Converter With STEVAL-ISA211V1*. STMicroelectronics. Accessed: Sep. 14, 2023. [Online]. Available: www.st.com

[32] C. Adragna and G. Gattavari. (Dec. 1999). *AN1215: How to Handle Short Circuit Conditions with ST's Advanced PWM Controllers*. STMicroelectronics. Accessed: Sep. 7, 2023. [Online]. Available: www.st.com

[33] J. Picard. (2011). *Power Supply Design Seminar: Under the Hood of Flyback SMPS Designs*. Texas Instruments Inc. Accessed: Sep. 7, 2023. [Online]. Available: www.ti.com

[34] H. Choi, "Flyback converter protection scheme with a selective shutdown delay time," in *Proc. IECON - 32nd Annu. Conf. IEEE Ind. Electron.*, Nov. 2006, pp. 2192–2196, doi: 10.1109/IECON.2006.347403.

[35] H.-S. Choi and D. Y. Huh, "Protection schemes for various fault conditions for off-line flyback converters," in *Proc. IEEE 35th Annu. Power Electron. Spec. Conf.*, Jun. 2004, pp. 4355–4359, doi: 10.1109/PESC.2004.1354770.

[36] P.-L. Huang, D. Chen, C.-J. Chen, and Y.-M. Chen, "An adaptive high-precision overpower protection scheme for primary-side controlled flyback converters," *IEEE Trans. Power Electron.*, vol. 26, no. 10, pp. 2817–2824, Oct. 2011, doi: 10.1109/TPEL.2011.2106223.

[37] *SIMetrix/SIMPLIS ver. 9 Advanced Power System Simulation*, Software (Commercial), Simplis Technologies Inc, Portland, OR, usa, 2022.

[38] *T3EL150302P Programmable DC Electronic Load*, User Manual, Teledyne-LeCroy, NY, USA, 2020.

[39] *Outline of Investigation for Wireless Power Transfer Equipment for Electric Vehicles, Edition 1*, document UL 2750, UL LLC, Mar. 2020.

[40] *Electric Vehicle Wireless Power Transfer (WPT) Systems—Part 1: General Requirements*, document IEC 61980-1:2020, Nov. 2020.

[41] *Electric Vehicle Wireless Power Transfer (WPT) Systems—Part 3: Specific Requirements for Magnetic Field Wireless Power Transfer Systems*, document IEC 61980-3:2022C Nov. 2022.

[42] Datasheet. (Oct. 2016). *ATL431, ATL432 2.5-V Low Iq Adjustable Precision Shunt Regulator*. TI. Accessed: Mar. 19, 2022. [Online]. Available: www.ti.com

[43] S. Cannenterre and C. Basso, "Quasi-resonant valley lockout without feedback reference," U.S. Patent 10 056 842 B2, Aug. 21, 2018. Accessed: Sep. 14, 2023. https://patents.google.com/patent/US10056842B2/

[44] S. Cannenterre and C. Basso, "Quasi-resonant valley lockout without feedback reference," U.S. Patent 10 355 606 B2, Jul. 16, 2019. Accessed: Sep. 14, 2023. [Online]. Available: https://patents.google.com/patent/US10355606B2/

[45] Quick Start Guide. (2019). *Bode 100 Vector Network Anlyzer*. OMICRON Lab. Accessed: May 22, 2022. [Online]. Available: www.omicron-lab.com

[46] C. Basso, *Switch-Mode Power Supplies: Spice Simulations and Practical Designs*, 2nd ed. New York, NY, USA: McGraw-Hill, 2014.

[47] C. Basso, *Transfer Functions of Switching Converters*, 1st ed. Los Angeles, CA, USA: Faraday Press, 2021.

[48] *FidoCadJ—A Free Graphical Editor for Electronics, Ver. 0.2.47*, Software (Free), Boston, MA, USA, 2021.

[49] *GNU Octave—A High-Level Interactive Language for Numerical Computations, Ver. 6.2.0*, Software (Free), Boston, MA, USA, 2021.

[50] *Libre Office Draw, ver. 6.2.5.x*, Software (Free), Boston, MA, USA, 2021.

[51] *Zotero ver. 6.0.x*, Software (Free), Corporation for Digital Scholarship, Vienna, VA, USA, Apr. 2022.

DARKO Đ. VRAČAR (Senior Member, IEEE) received the Dipl.-Ing., Magister, and Ph.D. degrees in electrical engineering from the School of Electrical Engineering, University of Belgrade, Serbia, in 2000, 2007, and 2023, respectively. His major field of study was power converters and drives.

He is currently a Senior Staff Engineer with BRUSA Elektronik (München) GmbH, Munich, Germany. He has 23 years of industrial experience and spent some time with companies, such as Delta, ABB, and Huawei Technologies. Some areas of expertise are the implementation of telecom and data center power supplies, and research and development of power electronics systems, such as solar inverters and SMPS for industrial and automotive applications. He has published several articles related to power converters and drives and holds one patent in power conversion systems. His research interests include simulation, control, and design of power converters. In addition, he was delivering training sessions and tutorials related to power electronics or industrial standards.

Dr. Vračar is a member of the following IEEE Societies: Industry Applications, Industrial Electronics, Power Electronics, Circuits and Systems, and Electromagnetic Compatibility.